Online ISSN 1848-3380, Print ISSN 0005-1144
ATKAFF 54(1), 89–102(2013)

Vinko Lešić, Mario Vašak, Nedjeljko Perić, Gojko Joksimović, Thomas M. Wolbank

Fault-tolerant Control of a Wind Turbine with Generator Stator Inter-turn Faults

DOI 10.7305/automatika.54-1.325
UDK 681.5.015.44.09-53; 621.313.52-85.04
IFAC 3.2; 2.1.4

Original scientific paper

Faults of wind turbine generator electromechanical parts are common and very expensive. This paper introduces a generator fault-tolerant control scheme for variable-speed variable-pitch wind turbines that can be applied regardless to the AC generator used. The focus is on generator stator isolation inter-turn fault that can be diagnosed and characterised before triggering the safety device. An extension of the conventional wind turbine control structure is proposed that prevents the fault propagation while power delivery under fault is deteriorated as less as possible compared to healthy machine conditions. Fault-induced and inherent asymmetries of the generator are estimated and respected by the field-oriented control of the generator to eliminate torque oscillations. An approach for asymmetry detection based on an unscented Kalman filter is proposed. Presented fault-tolerant control strategy is developed taking into account its modular implementation and installation in available control systems of existing wind turbines to extend their exploitable life span and increase energy production. Simulation results for the case of a megawatt class wind turbine are presented.

Key words: Wind turbine control, Generator fault-tolerant control, Stator winding isolation fault, Nonlinear estimation, Asymmetric field-oriented control

Upravljanje vjetroagregatom otporno na međuzavojske kvarove statorskog namota generatora. Kvarovi elektromehaničkih dijelova generatora vjetroagregata česti su i izrazito skupi. U ovom radu predstavljen je koncept na kvarove otpornog upravljanja generatorom vjetroagregata s promjenjivom brzinom vrtnje i zakretom lopatica primjenjiv bez obzira na tip korištenog izmjeničnog generatora. Naglasak je stavljen na oštećenje izolacije unutar namota jedne faze statora generatora koje se može dijagnosticirati i okarakterizirati prije aktiviranja sustava zaštite. Predložena je nadogradnja postojećeg sustava upravljanja vjetroagregatom koja sprječava širenje kvara i pritom postiže čim manje smanjenje proizvodnje električne energije u odnosu na normalan režim rada. Također je prikazano vektorsko upravljanje generatorom koje uzima u obzir nesimetrije generatora, kako one nastale uslijed djelovanja kvara, tako i one inherentne. U radu je prikazan pristup za otkrivanje nesimetrija generatora zasnovan na nederivacijskom Kalmanovu filtru. Predstavljena strategija upravljanja razvijena je uvažavajući mogućnost modularnog nadovezivanja na postojeće algoritme upravljanja već postavljenih vjetroagregata s ciljem produženja njihova životnog vijeka i povećanja proizvodnje energije. Dani su simulacijski rezultati za slučaj vjetroagregata iz megavatne klase.

Ključne riječi: upravljanje vjetroagregatom, upravljanje otporno na kvarove generatora, kvar izolacije statorskog namota, nelinearna estimacija, vektorsko upravljanje nesimetričnim strojem

1 INTRODUCTION

Increasing interest in renewable energy sources and their growing impact on today's energy production motivated different branches of science to make contributions in price reduction, energy quality and market competence of renewables. After a huge breakthrough and an average growth rate of 26% in last 5 years, wind energy today is a well-established technology with total world installed capacity of approximately 238 GW at the end of 2011 [1].

Remote locations are best suitable for wind turbines operation because of low-turbulent and strong winds. This introduces difficult and expensive maintenance procedures and rises availability concerns. Several fault-tolerant control algorithms have been introduced in [2] and they mostly propose different kinds of redundancies for sensors and electronic components. Focus here is on generator electromechanical faults, which are besides gearbox and power converters faults the most common in wind turbine systems [3]. Following the rising share of direct-drive wind

turbines (18% of the market in 2010 [1]) and thereby the usage of more complex and more fault-prone generators, the focus on generator faults in wind turbines is expected to further increase.

Due to the lowest failure rate among all kinds of machines [3], many already installed wind turbines have a squirrel-cage induction generator (SCIG). In our recent papers [4] and [5] we proposed a general idea of fault-tolerant control algorithm for generator electromechanical faults and its application in suppressing the rotor-bar defect in SCIGs. Algorithm is based on proper extension of widely adopted control strategies used in wind turbines, mainly on torque control loop with field-oriented control (FOC).

Focus of this paper is to research and develop a fault-tolerant control strategy for stator winding isolation faults that cause about 30% of machine faults [6–11] and are common for both asynchronous and synchronous machines used in wind turbines (doubly-fed induction generator, squirrel-cage induction generator, synchronous generator with wound rotor, synchronous generator with permanent magnets). A modulation of the generator flux using already available control system is introduced in order to suppress the fault propagation and to keep the electrical energy production possible under emergency circumstances.

There are two main issues connected with stator flux modulation for suppressing stator isolation faults:

- very slow dynamics of rotor-flux transients,
- modulation procedure needs to be performed with the high frequency of voltage supplied to the machine stator.

Another undesirable effect of machine electromechanical faults is the introduction of additional asymmetries in the machine. Stator inter-turn short circuit affects the magnetizing flux in the machine air-gap and causes appreciable torque oscillations. This degrades whole wind turbine system performance and, depending on the generator mounting in the nacelle, possibly enhances material fatigue. A method based on variable leakage inductance that takes into account machine asymmetries in the FOC procedure is proposed in [12]. An approach of utilizing the existing FOC variables estimation algorithm to include asymmetry detection based on an unscented Kalman filter is proposed. This paper applies the proposed method for the case of stator inter-turn isolation fault and achieves smooth generator operation in the faulty conditions. A similar work related to the asymmetries caused by SCIG rotor-bar faults is [13].

This paper is organized as follows. Section 2 presents the mathematical model of a variable-speed variable-pitch wind turbine, as well as its most-widely-adopted control strategy. The stator inter-turn isolation fault is briefly described in Section 3. In Section 4 a mathematical model of an SCIG is described explaining the theoretical basis used to form the wind turbine control system extension. A fault-tolerant approach and control algorithm that enables wind turbine operation under stator isolation fault is proposed and described in Section 5. A method for obtaining FOC variables based on unscented Kalman filter is presented in Section 6. Control of induction machine that improves asymmetric machine performance is described in Section 7. Section 8 provides simulation results for the case of 700 kW wind turbine.

2 WIND TURBINE CONTROL SYSTEM

Modern variable-speed variable-pitch wind turbines operate in two different regions. One is so-called low-wind-speed region where torque control loop adjusts the generator torque to achieve desired wind turbine rotational speed in order to make the power production optimal. The other region is high-wind-speed region where the power output is maintained constant while reducing the aerodynamic torque and keeping generator speed at the rated value. For this task a blade-pitch control loop is responsible. Both control loops are shown in Fig. 1

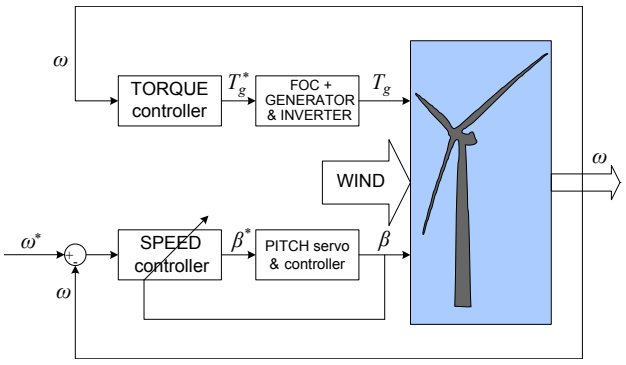

Fig. 1. Control system of a variable-speed variable-pitch wind turbine

The ability of a wind turbine to capture wind energy is expressed through a power coefficient C_P which is defined as the ratio of extracted power P_t to wind power P_V:

$$C_P = \frac{P_t}{P_V}. \tag{1}$$

The maximum value of C_P, known as Betz limit, is $C_{Pmax} = \frac{16}{27} = 0.593$. It defines the maximum theoretical capability of wind power capture. The real power coefficient of modern commercial wind turbines reaches values of about 0.48 [14]. Power coefficient data is usually given as a function of the tip-speed-ratio λ and pitch angle β

(Fig. 2). Turbine power and torque are given by [15], [16]:

$$P_t = C_P(\lambda,\beta)P_V = \frac{1}{2}\rho R^2 \pi C_P(\lambda,\beta)V^3, \quad (2)$$

$$T_t = \frac{P_t}{\omega} = \frac{1}{2}\rho R^3 \pi C_Q(\lambda,\beta)V^2, \quad (3)$$

where $C_Q = C_P/\lambda$, ρ, R, V and ω are torque coefficient, air density, radius of the aerodynamic disk of a wind turbine, wind speed and the angular speed of blades, respectively, and $\lambda = \frac{\omega R}{V}$. For more information about wind turbine modelling and control system design see [14–17].

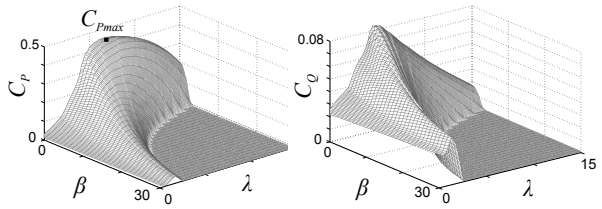

a) b)

Fig. 2. Power a) and torque b) coefficients for an exemplary 700 kW variable-pitch turbine

3 STATOR ISOLATION FAULT

Some of the most common causes of stator isolation faults are moisture in the isolation, winding overheating, or vibrations (especially due to fallen stator slot wedge). Modern voltage-source inverters also introduce additional voltage stress on the inter-turn isolation caused by the steep-fronted voltage surge [7], [8].

There are two main kinds of stator faults (Fig. 3). One is the isolation fault and short circuit between two different machine phases. The time elapsed between fault occurrence and triggered safety device is about one third of a second. If there is a short circuit between turns of the same phase the time elapsed between incipient fault and triggered safety device is about several minutes or even much longer, depending on the stator winding method [9]. This may give enough time for fault detection and adequate autonomous reaction provided by control system to suppress the fault from further spreading on other generator and wind turbine components.

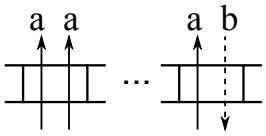

Fig. 3. Sketch of a stator slot including two turns of the same phase (aa) and two turns of different phases (ab)

The fault is manifested as a shorted turn in the phase winding with very low resistance. It results in high currents that flow through that turn and cause machine torque reduction and local overheating. The goal of considered fault-tolerant control is to keep the current in the shorted turn below its rated value and stop the fault from spreading on other components. This causes the wind turbine to operate at below-rated power but protects the generator until scheduled repair. This is very important for remotely-located wind turbines since the shorted turns induce local overheating and further spreading of the fault up to the point where the whole generator needs to be replaced.

The change of stator resistances due to occurred inter-turn fault is negligible (below 1% change). The change in fundamental wave inductances is also very small (1-2% change), however, it has a noticeable effect on the instantaneous value of the leakage inductance. The leakage inductance comprises all fundamental wave inductances masked in a mutual product and therefore results in much greater change (up to 10%), which can be observed with a fault-detection algorithm. Shorted phase has its own resistance and inductance and affects the main flux in the machine air-gap. Detection procedure developed in [10] is based on observing these changes at transient excitation caused by inverter pulses.

4 MATHEMATICAL MODEL OF AN INDUCTION MACHINE

Mathematical model of an AC squirrel-cage induction machine can be represented in the two-phase (d,q) rotating coordinate system [18–20]:

$$\bar{u}_s = R_s\bar{i}_s + \frac{\mathrm{d}\bar{\psi}_s}{\mathrm{d}t} + j\omega_e\bar{\psi}_s, \quad (4)$$

$$0 = R_r\bar{i}_r + \frac{\mathrm{d}\bar{\psi}_r}{\mathrm{d}t} + j(\omega_e-\omega_r)\bar{\psi}_r, \quad (5)$$

where bar notation represents a complex (d,q) vector, subscript s stator variables, subscript r rotor variables, i currents and R resistances. In a common rotating coordinate system stator variables are rotating with speed $\omega_e = 2\pi f$ and rotor variables with speed $\omega_e - p\omega_g$, where f is the frequency of the AC voltage supplied to the stator, ω_g is the speed of rotor, and p is the number of machine pole pairs. Flux linkages $\bar{\psi}_s$ and $\bar{\psi}_r$ are given by:

$$\bar{\psi}_s = L_s\bar{i}_s + L_m\bar{i}_r, \quad (6)$$

$$\bar{\psi}_r = L_m\bar{i}_s + L_r\bar{i}_r, \quad (7)$$

where $L_s = L_{s\sigma} + L_m$ is stator inductance, $L_r = L_{r\sigma} + L_m$ is rotor inductance, and L_m is mutual inductance. Parameters $L_{s\sigma}$ and $L_{r\sigma}$ are stator and rotor flux leakage inductances, respectively.

By perturbing relations (4)-(7) and by fixing the rotor flux linkage to d axis ($\bar{\psi}_r = \psi_{rd}$), a rotor field-oriented control (RFOC) equations are obtained:

$$i_{mr} = \frac{\psi_{rd}}{L_m}, \tag{8}$$

$$i_{sd} = i_{mr} + T_r \frac{\mathrm{d}i_{mr}}{\mathrm{d}t}, \tag{9}$$

$$\omega_{sl} = \omega_e - p\omega_g, \tag{10}$$

$$T_g = \frac{3}{2} p \frac{L_m^2}{L_r} i_{mr} i_{sq} = k_m i_{mr} i_{sq}, \tag{11}$$

where i_{mr} is the magnetizing current that creates the rotor flux, $T_r = \frac{L_r}{R_r}$ is the rotor time constant, $\omega_{sl} = \frac{i_{sq}}{T_r i_{mr}}$ is the slip speed and T_g is the electromagnetic torque. The torque is controlled only by q stator current component because magnetizing current vector i_{mr} is dependent on the time lag T_r and is therefore kept constant in the sub-nominal speed operating region.

Voltage-controlled machine (Fig. 4) is usually more suitable than the current-controlled so by eliminating ψ_s and i_r, and by introducing (8) in (4)-(7), stator voltage vector components u_{sd} and u_{sq} are obtained:

$$u_{sd} = k_s i_{sd} + L_l \frac{\mathrm{d}i_{sd}}{\mathrm{d}t} + \left(\frac{L_l}{T_r} - \frac{L_s}{T_r} \right) i_{mr} - \omega_e L_l i_{sq}, \tag{12}$$

$$u_{sq} = R_s i_{sq} + L_l \frac{\mathrm{d}i_{sq}}{\mathrm{d}t} - \omega_e \left(L_l - L_s \right) i_{mr} + \omega_e L_l i_{sd}, \tag{13}$$

where $L_l = (L_s - \frac{L_m^2}{L_r})$ and $k_s = (R_s - \frac{L_l}{T_r} + \frac{L_s}{T_r})$. Parameter L_l denotes the leakage inductance. Relations (12) and (13) show that d and q coordinates are not fully decoupled and changing the voltage value in one axis affects also the other. By introducing correction voltages Δu_{sd} and Δu_{sq}, fully decoupled relations are derived:

$$u_{sd} + \Delta u_{sd} = k_s i_{sd} + L_l \frac{\mathrm{d}i_{sd}}{\mathrm{d}t}, \tag{14}$$

$$u_{sq} + \Delta u_{sq} = R_s i_{sq} + L_l \frac{\mathrm{d}i_{sq}}{\mathrm{d}t}, \tag{15}$$

with

$$\Delta u_{sd} = \frac{1}{T_r} \frac{L_m^2}{L_r} i_{mr} + \omega_e L_l i_{sq}, \tag{16}$$

$$\Delta u_{sq} = -\omega_e \frac{L_m^2}{L_r} i_{mr} - \omega_e L_l i_{sd}. \tag{17}$$

These equations are now suitable for further design of the control loop and proportional-integral (PI) controllers are chosen with integral time constants $T_{Id} = L_l/k_s$ for d-current, $T_{Iq} = L_l/R_s$ for q-current and gain K_r. Finally, closed loop dynamics can now be represented as a first-order lag system with transfer function:

$$\frac{i_{sd}(s)}{i_{sd}^*(s)} = \frac{i_{sq}(s)}{i_{sq}^*(s)} = \frac{1}{1 + \tau s}, \tag{18}$$

where τ is a time constant defined with $\tau = \frac{L_l}{K_r}$.

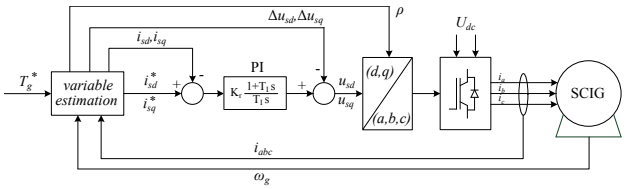

Fig. 4. Field-oriented control loop

5 FAULT-TOLERANT CONTROL

In order to stop the fault from spreading the current flowing through shorted turns must be kept below nominal value, as stated before. The current flow is caused by induced voltage due to variable magnetic flux. Therefore the current can be restricted with manipulation of magnetic flux. In the three-phase coordinate system (a, b, c) stator voltage equation is defined with:

$$u_{sx} = i_{sx} R_s + \frac{\mathrm{d}\psi_{sx}}{\mathrm{d}t} \approx \frac{\mathrm{d}\psi_{sx}}{\mathrm{d}t}, \tag{19}$$

where x denotes one of the phases. Generally, the stator flux is considered sine-wave (in the fundamental-wave approaches, such as FOC) with amplitude $|\psi_s|$, angular frequency ω_e and phase offset φ_x. The flux in phases a, b, c is represented with:

$$\psi_{sx}(t) = |\psi_s|(t) \sin(\omega_e t + \varphi_x). \tag{20}$$

Flux amplitude envelope denoted with $|\psi_s|(t)$ in (20) is time-variable and must be taken into account when calculating the flux derivative for fault suppression:

$$\frac{\mathrm{d}\psi_{sx}(t)}{\mathrm{d}t} = \frac{\mathrm{d}|\psi_s|(t)}{\mathrm{d}t} \sin(\omega_e t) + |\psi_s|(t) \omega_e \cos(\omega_e t). \tag{21}$$

The goal for suppressing the fault is formed as a restricted value of flux derivative:

$$\left| \frac{\mathrm{d}\psi_{sx}}{\mathrm{d}t} \right| \leq k. \tag{22}$$

The value k is determined based on fault identification procedure through machine fault monitoring and characterisation techniques [10]. Following from (19) this restricts the induced voltage in the faulted turns and consequently also the circulating currents responsible for local overheating.

Considering the design of fault-tolerant control strategy, one approach is to keep $|\psi_s|$ constant at the nominal value and use wind turbine pitch control to restrict ω_g and consequently ω_e never to exceed maximum allowed value defined with product $|\psi_s|\omega_e$ (Fig. 5, *Faulty A* waveform). Other approach is to use constant but weakened flux ψ_s such that $|\psi_s|\omega_e$ is kept below value of k. Wind turbine

pitch control is again used to lower the aerodynamic torque in order to impose the torque balance. The weakened flux is shown in Fig. 5 as *Faulty B* waveform. In both cases, flux amplitude is kept constant at some value. Both approaches lower the generator power production significantly and possibly unnecessarily. In the sequel we present a method for significantly improving the wind turbine power production while suppressing the fault at the same time.

From (22) it follows that in order to stop the fault from spreading, the stator flux waveform must never be allowed to exceed a restriction shaped as a triangular waveform $|kt|$ shown in Fig. 5 (dash-dot). The restriction also represents the flux waveform that enables maximum power production in the faulty machine state. Therefore, our goal is to utilize the existing control strategy and FOC to achieve that triangular waveform.

An appropriate flux amplitude envelope is chosen such that $\left|\frac{\mathrm{d}\psi_{sx}}{\mathrm{d}t}\right| = k$ is ensured (for phase a with $\varphi_a = 0$):

$$|\psi_s|(t) = \frac{\frac{k}{\omega_e}\omega_e t}{\sin(\omega_e t)}, \tag{23}$$

with minimum absolute value at angles $\omega_e t = 0, \pi, ...$, and maximum at $\omega_e t = \pi/2, 3\pi/2...$:

$$\begin{array}{rcl} |\psi_s|(0) & = & \frac{k}{\omega_e}, \\ |\psi_s|\left(\frac{\pi}{2}\right) & = & \frac{k}{\omega_e}\frac{\pi}{2}. \end{array} \tag{24}$$

With modulated amplitude (23) the flux waveform from (20) obtains the form:

$$\begin{array}{rcll} \psi_{sa}(t) & = & kt, & t \in [-\frac{\pi}{2\omega_e}, \frac{\pi}{2\omega_e}] \\ \psi_{sa}(t) & = & -kt + k\pi, & t \in [\frac{\pi}{2\omega_e}, \frac{3\pi}{2\omega_e}] \end{array} \tag{25}$$

Transformed to the (d, q) and RFOC domain, stator flux linkage is defined with $\bar{\psi}_s = \psi_{sd} + j\psi_{sq}$ where:

$$\begin{array}{rcl} \psi_{sd} & = & L_l i_{sd} + \frac{L_m}{L_r}\psi_{rd}, \\ \psi_{sq} & = & L_l i_{sq}, \end{array} \tag{26}$$

and relation $|\psi_s| = \sqrt{\psi_{sd}^2 + \psi_{sq}^2}$ holds.

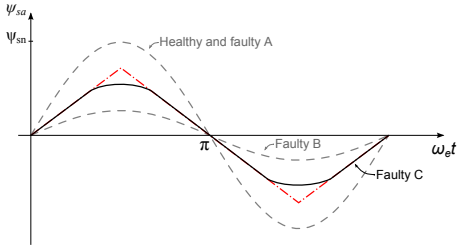

Fig. 5. Stator flux waveforms for healthy and faulty machine

Changing the ψ_{rd} is very slow due to large rotor time-lag T_r, so we choose to manipulate the flux ψ_{sx} only through machine fast dynamics (18). Proper values of current components i_{sd} and i_{sq} are chosen to achieve the triangular form in Fig. 5 while taking into account that $|i_s|$ must not exceed predefined nominal value i_{sn}. With this approach, minimum and maximum achievable fluxes are for the case when i_{sq} is set to zero and i_{sd} to rated value of machine stator currents amplitude $\mp i_{sn}$:

$$\psi_{s\_min,max} = \mp L_l i_{sn} + \frac{L_m}{L_r}\psi_{rd}. \tag{27}$$

However, desired machine torque and corresponding i_{sq} must also be included into consideration. Due to saturation, the maximum flux is also restricted with the rated value of the stator flux. The value of ψ_{rd} is considered constant during the manipulation of stator flux. In practice it is influenced by changing the i_{sd} current and it slowly fluctuates around mean value of the chosen ψ_{rd}.

If parameter k from the fault condition (22) is too large or chosen ψ_{rd} value limits the freedom for desired fast dynamics, desired amplitude scope shown in Fig. 6 with peak values (24) is not achievable. Therefore the minimum value is set to ψ_{s_min} and when the amplitude envelope $|\psi_s|(t)$ reaches value of ψ_{s_max} (at time instant t_m) it is fixed to that value. Stator flux takes the form presented as *Faulty C* in Fig. 5. The amplitude envelope is shown in Fig. 6 with dashed line representing the case when triangular waveform is achievable and full line for the case of *Faulty C* waveform. The time instant t_m can be obtained from condition:

$$kt_m = \psi_{s\_max}\sin(\omega_e t_m). \tag{28}$$

Considering (21), influence of the static part $|\psi_s|(t)\omega_e\cos(\omega_e t)$ of equation is examined. Derivative of flux amplitude envelope (23) from Fig. 6 is:

$$\frac{\mathrm{d}|\psi_s|(t)}{\mathrm{d}t} = k\frac{\sin(\omega_e t) - \omega_e t\cos(\omega_e t)}{\sin^2(\omega_e t)}. \tag{29}$$

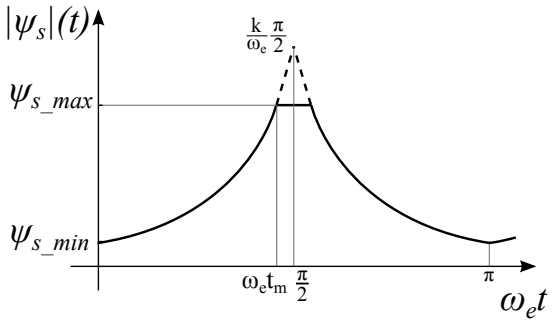

Fig. 6. Flux amplitude from (23) *for achieving* $\left|\frac{\mathrm{d}\psi_s}{\mathrm{d}t}\right| \leq k$

The flux amplitude derivative reaches its maximum value of k at time instant $t = \frac{\pi}{2\omega_e}$. By putting (23) and (29) into (21) the condition (22) is satisfied.

As the q-current is responsible for maintaining the constant torque, the d-current dynamics determines, according to (26), the dynamics of $|\psi_s|(t)$. Fastest achievable transient of i_{sd} is determined with inverter limitation. Considering the worst case scenario and a typical value of U_{dc} in wind turbines, even the maximum stator flux derivative at $t = \frac{\pi}{2\omega_e}$ is achievable and this issue is not explicitly treated in the derived FTC.

Desired generator torque reference T_g^* dictated by the wind turbine torque control loop determines adequate value of ω_e and i_{mr} (or ψ_{rd}) used to achieve correct ψ_{s_min} and ψ_{s_max}. Current references i_{sd}^* and i_{sq}^* are then calculated to obtain desired stator flux wave. The algorithm is given in the Algorithm 1 and schematically in Fig. 7.

Algorithm 1 Fault-tolerant control for stator isolation fault

1. Calculate stator flux mean value ψ_{s_mean} from Fig. 6, corresponding i_{mr_mean} and i_{sq_mean} using (10), (11) and (26) with instantaneous torque reference T_g^*, steady state condition $i_{sd} = i_{mr}$ and rated slip condition $\omega_{sl} = \omega_{sln}$;
2. Obtain ω_e from (10) and instantaneous speed ω_g;
3. Obtain ψ_{s_min} from (24);
4. If obtained $\psi_{s\_mean} < \psi_{s\_min}$ apply simple flux weakening method with $i_{sd}^* = i_{mr\_mean}$, else apply the flux modulation:
5. Find t_m and ψ_{s_max} from obtained ψ_{s_mean} and (23);
6. Apply $i_{sd}^*(t)$ calculated from k, ω_e, ψ_{s_max}, (23) and (26); apply $i_{sq}^*(t)$ calculated from T_g^*, i_{mr_mean} and (11);
7. **Initialization of FTC:** Set $\omega_{g1} = \omega_{gn}$ and execute steps 1-6 until $\psi_{s\_max} \leq \frac{k}{\omega_e}\frac{\pi}{2}$ from (24). Decrease ω_{g1} by small value ϵ_ω at each iteration; set ω_g^* equal to the obtained ω_{g1} at the last iteration.

For less computational effort, step 6 is executed at each discrete time step while steps 1-5 are executed once in every stator flux modulation period (Fig. 6). Steps 1-5 require solving of simple algebraic equations i.e. quadratic and square root equations but can be simplified even more by using look-up tables. Initialization of the algorithm is executed only once when a fault is diagnosed and can also be obtained from look-up table $\omega_{g1}(k)$.

Using the described method, an exemplary graph of available speed-torque points under machine fault is shown in Fig. 8. Normal operation of the healthy generator is bounded with rated machine torque T_{gn} and rated speed ω_{gn} and pitch control is responsible to keep the operating point between boundaries. The curve denoted with *Optimum power* represents optimal operating points of wind turbine at which the power factor coefficient C_p and power production is at maximum value.

For the case of diagnosed fault, dashed area denotes all available generator torque values that can be achieved for certain generator speed. Generator torque denoted with T_f is the largest available torque that can be achieved under fault condition for certain speed. Below speed ω_g^* generator is operating in the safety region and no fault-tolerant control is needed. It follows that up to the speed ω_{g1} it is possible to control the wind turbine in the faulty case without sacrificing power production. However, from that speed onwards it is necessary to use blades pitching in order to limit the aerodynamic torque and to keep the power production below optimal in order to suppress the fault from spreading. The speed control loop is modified such that instead of reference ω_{gn} the reference ω_{g1} is selected. Interventions in classical wind turbine control that ensure fault-tolerant control are given in Fig. 9.

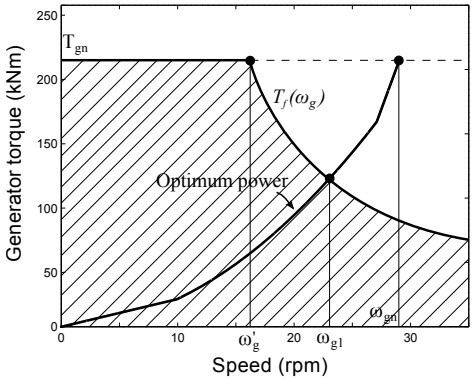

Fig. 8. Available torque-speed generator operating points under fault condition (shaded area)

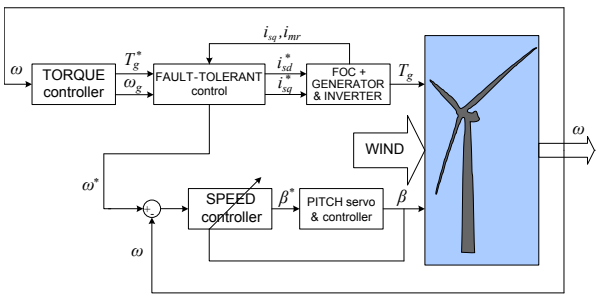

Fig. 9. Control system of wind turbine with fault-tolerant control strategy

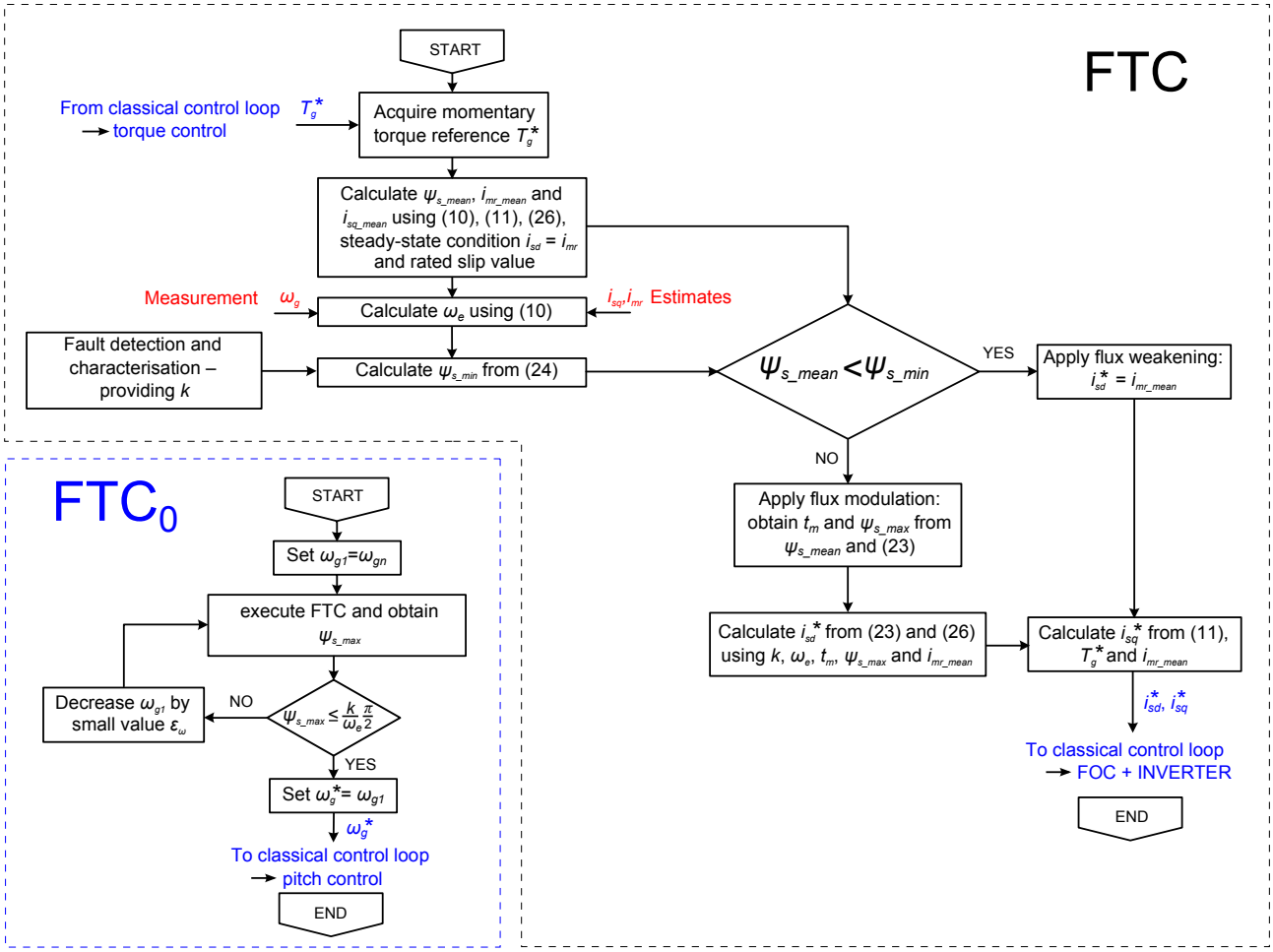

Fig. 7. State flow of the FTC algorithm and algorithm initialization FTC_0 (Step 7 in Algorithm 1)

6 ESTIMATION OF FIELD-ORIENTED CONTROL VARIABLES

In this paper a dual unscented Kalman filter (UKF) is used for FOC variables estimation because of its proficient ability to cope with hard nonlinearities. The UKF represents a novel approach for estimations in nonlinear systems and provides better results than extended Kalman filter (EKF) in terms of mean estimate and estimate covariance [21].

The core idea of UKF lies in unscented transformation, way of representing and propagating Gaussian random variables (GRV) through a nonlinear mapping. The unscented transformation enables better capturing of mean and covariance of GRVs than simple point-linearization of the mapping: posterior mean and covariance are accurate to the second order of the Taylor series expansion for any nonlinearity. More information about the unscented Kalman filter theory can be found in [21] and [22] while different applications of UKF are presented in [23–25].

6.1 Stochastic induction machine model

Machine model states in common (d, q) reference frame are i_{sd} and i_{sq} stator currents, magnetizing current i_{mr} and position of the magnetic flux ρ. Mathematical model used for state estimation of the symmetric machine via UKF is:

$$\frac{\mathrm{d}i_{sd}}{\mathrm{d}t} = \frac{1}{L_l}u_{sd} + \frac{1}{L_l}\Delta u_{sd} - \frac{k_s}{L_l}i_{sd} + v_1, \quad (30)$$

$$\frac{\mathrm{d}i_{sq}}{\mathrm{d}t} = \frac{1}{L_l}u_{sq} + \frac{1}{L_l}\Delta u_{sq} - \frac{R_s}{L_l}i_{sq} + v_2, \quad (31)$$

$$\frac{\mathrm{d}i_{mr}}{\mathrm{d}t} = \frac{1}{T_r}\left(i_{sd} - i_{mr}\right) + v_3, \quad (32)$$

$$\frac{\mathrm{d}\rho}{\mathrm{d}t} = p\omega_g + \frac{1}{T_r}\frac{i_{sq}}{i_{mr}} + v_4, \quad (33)$$

where variables $v_{1,..,4}$ denote process noise.

For reliable estimation of i_{sd} and i_{sq} currents, the dependency on flux angle ρ has to be included in relations

(30) and (31). It can be done by introducing line voltages in (a,b,c) coordinate system and by applying Park's and Clark's transform [18], which results in:

$$\begin{aligned} u_{sd} &= \tfrac{2}{3}u_{ab}\ \cos\rho + \left(\tfrac{1}{3}\cos\rho + \tfrac{\sqrt{3}}{3}\sin\rho\right)u_{bc}, \\ u_{sq} &= -\tfrac{2}{3}u_{ab}\ \sin\rho + \left(-\tfrac{1}{3}\sin\rho + \tfrac{\sqrt{3}}{3}\cos\rho\right)u_{bc}. \end{aligned} \tag{34}$$

Inputs vector for the UKF is therefore chosen to include line voltages coming out from FOC and measured generator speed:

$$u = \left[u_{ab}\ \ u_{bc}\ \ \omega_g\right]^T. \tag{35}$$

Stator currents are usually measured in electrical machine applications and they are therefore used in UKF states correction procedure. Since the state vector $x = [i_{sd}\quad i_{sq}\quad i_{mr}\quad \rho]^T$ is in (d,q) coordinates and measurements are in (a,b,c) coordinates, inverse Clark's and Park's transforms are applied and measurement vector is chosen as $y = [i_a\ \ i_b]^T$:

$$\begin{aligned} i_a =& i_{sd}\cos\rho - i_{sq}\sin\rho + n_1, \\ i_b =& i_{sd}\left(-\frac{1}{2}\cos\rho + \frac{\sqrt{3}}{2}\sin\rho\right) + \\ &+ i_{sq}\left(\frac{1}{2}\sin\rho + \frac{\sqrt{3}}{2}\cos\rho\right) + n_2, \end{aligned} \tag{36}$$

where n_1 and n_2 denote measurement noise.

6.2 Unscented Kalman filter algotithm

The UKF itself is shortly described next. The estimated state vector $\hat{x}_k$ in a discrete time-instant k is augmented to include means of process and measurement noise $\bar{v}$ and $\bar{n}$:

$$\hat{x}_k^a = \mathbb{E}(x_k^a) = \left[\hat{x}_k^T\ \ \bar{v}\ \ \bar{n}\right]^T, \tag{37}$$

where $\mathbb{E}(\cdot)$ denotes the expectation of a random variable. State covariance matrix $\mathbf{P}_k$ is also augmented accordingly:

$$\mathbf{P}_k^a = \mathbb{E}\left((x_k^a - \hat{x}_k^a)^T(x_k^a - \hat{x}_k^a)\right) = \begin{bmatrix} \mathbf{P}_k & \mathbf{0} & \mathbf{0} \\ \mathbf{0} & \mathbf{R}^v & \mathbf{0} \\ \mathbf{0} & \mathbf{0} & \mathbf{R}^n \end{bmatrix}, \tag{38}$$

where $\mathbf{R}^v$ and $\mathbf{R}^n$ are process and measurement noise covariance matrices, respectively. Time update algorithm starts with the unscented transformation and by forming the sigma points matrix $\mathcal{X}_k^a$:

$$\mathcal{X}_k^a = \left[\hat{x}_k^a \quad \hat{x}_k^a + \gamma\sqrt{\mathbf{P}_k^a} \quad \hat{x}_k^a - \gamma\sqrt{\mathbf{P}_k^a}\right]. \tag{39}$$

Variable $\sqrt{\mathbf{P}_k^a}$ is the lower-triangular Cholesky factorization of matrix $\mathbf{P}_k^a$ and $\gamma = \sqrt{L+\lambda}$ is a scaling factor. Parameter L is the dimension of augmented state x_k^a and parameter λ determines the spread of sigma points around the current estimate, calculated as:

$$\lambda = \alpha^2\left(L + \kappa\right) - L. \tag{40}$$

Parameter α is usually set to a small positive value e.g. $10^{-4} \leq \alpha \leq 1$ and κ is usually set to 1. There are $2L+1$ sigma points used for the transformation, which correspond to the columns in $\mathcal{X}_k^a = \left[(\mathcal{X}_k^x)^T\ \ (\mathcal{X}_k^v)^T\ \ (\mathcal{X}_k^n)^T\right]^T$.

Time-update equations used to calculate prediction of state $\hat{x}_{k+1}^-$ and state covariance $\mathbf{P}_{k+1}^-$ as well as prediction of output $\hat{y}_{k+1}^-$ are:

$$\mathcal{X}_{i,k+1|k}^x = F\left(\mathcal{X}_{i,k}^x, u_k, \mathcal{X}_{i,k}^v\right), \quad i = 0,...,2L, \tag{41}$$

$$\hat{x}_{k+1}^- = \sum_{i=0}^{2L} W_i^{(m)}\mathcal{X}_{i,k+1|k}^x, \tag{42}$$

$$\begin{aligned} \mathbf{P}_{k+1}^- = &\sum_{i=0}^{2L} W_i^{(c)}\left(\mathcal{X}_{i,k+1|k}^x - \hat{x}_{k+1}^-\right)\times \\ &\left(\mathcal{X}_{i,k+1|k}^x - \hat{x}_{k+1}^-\right)^T, \end{aligned} \tag{43}$$

$$\mathcal{Y}_{i,k+1|k} = H\left(\mathcal{X}_{i,k+1|k}^x, \mathcal{X}_{i,k}^n\right), \quad i = 0,...,2L, \tag{44}$$

$$\hat{y}_{k+1}^- = \sum_{i=0}^{2L} W_i^{(m)}\mathcal{Y}_{i,k+1|k}, \tag{45}$$

where i is the index of columns in matrix $\mathcal{X}_k^a$ (and also in $\mathcal{X}_k^x, \mathcal{X}_k^v, \mathcal{X}_k^n$) starting from value zero. Function $F(\cdot)$ is the model vector function from (30)-(33) where the next state is obtained by Runge-Kutta numerical integration. Function $H(\cdot)$ represent measurements from (36). Weights for mean and covariance calculations are given by:

$$\begin{aligned} W_0^{(m)} &= \tfrac{\lambda}{(L+\lambda)}, \\ W_0^{(c)} &= \tfrac{\lambda}{(L+\lambda)} + \left(1 - \alpha^2 + \beta\right), \\ W_i^{(m)} &= W_i^{(c)} = \tfrac{\lambda}{2(L+\lambda)}, \quad i = 1,...,2L. \end{aligned} \tag{46}$$

For Gaussian distributions, $\beta = 2$ is optimal.

Measurement update algorithm is performed in the similar way as in classical Kalman filter but requires also output covariance matrix $\mathbf{P}_{\tilde{y}_{k+1}\tilde{y}_{k+1}}$ and cross-covariance matrix $\mathbf{P}_{\tilde{x}_{k+1}\tilde{y}_{k+1}}$:

$$\begin{aligned} \mathbf{P}_{\tilde{y}_{k+1}\tilde{y}_{k+1}} = &\sum_{i=0}^{2L} W_i^{(c)}\left(\mathcal{Y}_{i,k+1|k} - \hat{y}_{k+1}^-\right)\times \\ &\left(\mathcal{Y}_{i,k+1|k} - \hat{y}_{k+1}^-\right)^T, \end{aligned} \tag{47}$$

$$\begin{aligned} \mathbf{P}_{\tilde{x}_{k+1}\tilde{y}_{k+1}} = &\sum_{i=0}^{2L} W_i^{(c)}\left(\mathcal{X}_{i,k+1|k}^x - \hat{x}_{k+1}^-\right)\times \\ &\left(\mathcal{Y}_{i,k+1|k} - \hat{y}_{k+1}^-\right)^T, \end{aligned} \tag{48}$$

followed by the correction of predicted states and covariance:

$$\mathbf{K}_{k+1} = \mathbf{P}_{\tilde{x}_{k+1}\tilde{y}_{k+1}}\mathbf{P}^{-1}_{\tilde{y}_{k+1}\tilde{y}_{k+1}}, \quad (49)$$

$$\hat{x}_{k+1} = \hat{x}^{-}_{k+1} + \mathbf{K}_{k+1}\left(y_{k+1} - \hat{y}^{-}_{k+1}\right), \quad (50)$$

$$\mathbf{P}_{k+1} = \mathbf{P}^{-}_{k+1} - \mathbf{K}_{k+1}\mathbf{P}_{\tilde{y}_{k+1}\tilde{y}_{k+1}}\mathbf{K}^{T}_{k+1}. \quad (51)$$

where $\mathbf{K}_k$ is Kalman gain matrix.

At the time-instant k measurement update is executed first. It results in current estimates which may be used for the control algorithm, i.e. to obtain the current input u_k. These two parts are time-critical in the on-line implementation. They are followed by time-update algorithm part which should be finished by the next sampling instant $(k+1)$ when new measurements arrive.

An attractive feature of UKF is that partial derivatives and Jacobian matrix (like in EKF) are not needed and continuous-time nonlinear dynamics equations are directly used in the filter, without discretization or linearization. Therefore, equations (30)-(33) and Runge-Kutta numerical integration algorithm are used for calculating predictions of states.

7 CONTROL OF ASYMMETRIC INDUCTION MACHINE

Assuming the fault is suppressed and machine can operate safely, influence of the modified flux and corresponding torque modulation due to shorted turns still remains. In Section 4 a widely-adopted RFOC algorithm is described. It provides very good results and satisfying performance of a nearly symmetrical machine. Several modifications can be applied to further improve its performance. Often applied one is to consider machine saliencies by choosing different values of stator inductances in d and q axes [18]. Also a lot of effort is currently put into finding adequate solution for sensorless drives [26, 27].

In the sequel, an RFOC algorithm for asymmetric machine is proposed. The algorithm is conceived as an extension of the previously described method for symmetric machine control.

7.1 Model of the asymmetry

For symmetric fundamental-wave machine the transient leakage inductance is the same for all phases and so far the parameter L_l was implied to be constant. Due to occurred asymmetry in the machine, the transient leakage inductance is no longer the same for all phases and can be represented with a complex value denoted with $\bar{L}_{l,t}$. It is composed of a scalar offset value L_{offset} and a complex value $\bar{L}_{mod}$. The offset value represents the symmetric part while complex value includes induced asymmetry with its magnitude and spatial direction. More about this approach can be found in [10, 28, 29]. In stator reference frame leakage inductance $L_{l,t}$ is represented as:

$$\bar{L}_{l,t} = L_{offset} + \bar{L}_{mod}, \qquad \bar{L}_{mod} = L_{mod}\cdot e^{j2\gamma}. \quad (52)$$

The angle $\gamma = \omega_e t + \varphi$ corresponds to the current location of the stator fault with respect to the magnetizing flux. The frequency is doubled due to effects of both north and south magnetic field poles per single flux revolution period.

Every machine in normal operation has inherent asymmetries, which are the result of spatial saturation, anisotropy, saliencies etc. The most conspicuous one is the saturation saliency that arises from the spatial distribution of the fundamental wave along the stator circumferences [10]. The period is also twice as of the fundamental wave. This particular inherent asymmetry is dependent on the flux magnitude and load amount and can be noticeable in normal machine operation. Another asymmetry is caused by slot openings in the rotor lamination and its period corresponds to the number of rotor bars.

For the fault detection procedure and machine diagnostics, it is important to segregate different causes of asymmetries and observe the influence of each. From the control viewpoint, the total leakage inductance is included in the control procedure as a representative value in which all contributions from different asymmetry causes are reflected in the fundamental-wave model, including the fault-induced ones.

7.2 Field-oriented control for asymmetric induction machine

By transferring to the common reference frame the leakage inductance can be represented with:

$$\bar{L}_{l,t} = L_{ld} + j\cdot L_{lq}, \quad (53)$$

where $L_{ld} = L_{offset} + L_{mod}\cos(2\gamma)$, and $L_{lq} = L_{mod}\sin(2\gamma)$.

The leakage inductance from (53) is put into induction machine stator and rotor voltage equations (4) and (5) and linear transformations of equalities are performed in the same manner as for the case of deriving conventional symmetric FOC equations. Result is the mathematical model of the asymmetric induction machine based on the variable

leakage inductance approach:

$$u_{sd} = k_a i_{sd} + L_a \frac{\mathrm{d}i_{sd}}{\mathrm{d}t} - \frac{L_{lq}}{L_{ld}} u_{sq} + \frac{L_{lq}}{L_{ld}} R_s i_{sq} - \\ - \omega_e L_a i_{sq} + \left(\frac{L_a}{T_r} - \frac{L_s}{T_r} \right) i_{mr} + \omega_e \frac{L_{lq}}{L_{ld}} L_s i_{mr}, \tag{54}$$

$$u_{sq} = R_s i_{sq} + L_a \frac{\mathrm{d}i_{sq}}{\mathrm{d}t} + \frac{L_{lq}}{L_{ld}} u_{sd} - \frac{L_{lq}}{L_{ld}} \left(R_s + \frac{L_s}{T_r} \right) i_{sd} + \\ + \omega_e L_a i_{sd} + \frac{L_{lq}}{L_{ld}} \frac{L_s}{T_r} i_{mr} - \omega_e (L_a - L_s) i_{mr}, \tag{55}$$

where $k_a = (R_s - \frac{L_a}{T_r} + \frac{L_s}{T_r})$ and $L_a = \left(L_{ld} + \frac{L_{lq}^2}{L_{ld}} \right)$. In the same way as in symmetric FOC, the decoupling method is applied. By introducing correction voltages Δu_{sd} and Δu_{sq}, fully decoupled relations are derived:

$$u_{sd} + \Delta u_{sd} = k_a i_{sd} + L_a \frac{\mathrm{d}i_{sd}}{\mathrm{d}t}, \tag{56}$$

$$u_{sq} + \Delta u_{sq} = R_s i_{sq} + L_a \frac{\mathrm{d}i_{sq}}{\mathrm{d}t}. \tag{57}$$

It may be observed that relations (56) and (57) have the same form as for the case of symmetric machine (14) and (15), and therefore the same controller structure can be applied. Decoupling voltages of the asymmetric machine model are:

$$\Delta u_{sd} = \frac{L_{lq}}{L_{ld}} u_{sq} - \frac{L_{lq}}{L_{ld}} R_s i_{sq} + \omega_e L_a i_{sq} - \\ - \left(\frac{L_a}{T_r} - \frac{L_s}{T_r} \right) i_{mr} - \omega_e \frac{L_{lq}}{L_{ld}} L_s i_{mr}, \tag{58}$$

$$\Delta u_{sq} = - \frac{L_{lq}}{L_{ld}} u_{sd} + \left(\frac{L_{lq}}{L_{ld}} R_s + \frac{L_{lq}}{L_{ld}} \frac{L_s}{T_r} \right) i_{sd} - \\ - \omega_e L_a i_{sd} - \frac{L_{lq}}{L_{ld}} \frac{L_s}{T_r} i_{mr} + \omega_e (L_a - L_s) i_{mr}. \tag{59}$$

Equations (54)-(59) represent the mathematical model for an asymmetric induction machine. With complex leakage inductance from (52) and (53), influence of the shorted phase is respected in machine control. Change of stator resistance R_s and inductance L_s due to inter-turn short-circuit is neglected as described in Section 3. With $L_{ld} = L_{offset} = L_l$ and $L_{lq} = 0$ above relations are valid for symmetric machine as well and they obtain the same form as in (12)-(17).

In the same manner, PI controller parameters are chosen with integral time constants $T_{Ida} = L_a/k_a$ for d-current, $T_{Iqa} = L_a/R_s$ for q-current. Index 'a' denotes controller parameters in case of detected asymmetry. PI controller gain K_{ra} is selected with respect to the desired transient velocity and inverter constraints. Control system block scheme remains the same as in Fig. 4.

The way of detecting the true value of leakage inductance $\bar{L}_{l,t}$ under asymmetric machine conditions determines how much the system performance is improved with the new FOC algorithm. A method of high-sensitive detection that is based on investigation of machine behavior on transient excitation caused by inverter switching is proposed in [29] and further developed in [10].

The FOC algorithm is based on precisely determined flux angle, which is needed for coordinate system transformations. Control algorithm therefore includes an observer and Kalman filter is one of the common approaches. With the goal of minimum modifications to the conventional FOC control algorithm, the existing Kalman filter is extended to provide estimation of the leakage inductance. By applying this approach, the minimum computational time increase is achieved.

7.3 Estimation of the variable transient leakage

For the purpose of simultaneous parameter estimation in the model (30)-(33), the UKF from Section 6 is extended into so-called dual UKF configuration. Parameters in the dual Kalman filter implementation approach are estimated with a separate filter (Fig. 10). This way two state vectors are formed: $x = [i_{sd} \quad i_{sq} \quad i_{mr} \quad \rho]^T$ and $\theta = [\theta_1 \quad \theta_2]^T$, where $\theta_1 = \varphi$ and $\theta_2 = L_{mod}$, and two estimation algorithms are executed sequentially at each sampling instant. Whole control system is presented in Fig. 11. An example of dual Kalman filter configuration well-known in electrical drives community is a 'braided' Kalman filter [30].

Magnetic flux rotational speed is calculated from states estimation using (10) and together with θ_1 location of the asymmetry γ in the (d, q) frame can be obtained. Considering (52) and (53), the complex value of $\bar{L}_{l,t}$ (and corre-

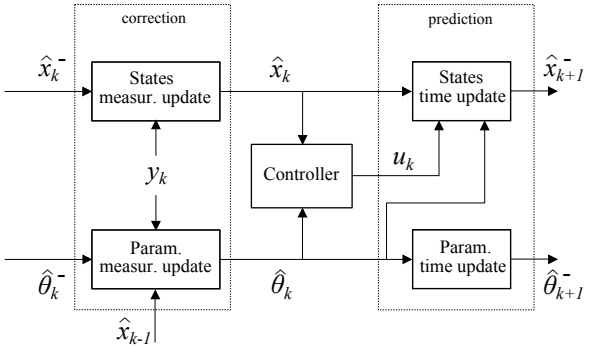

Fig. 10. Dual unscented Kalman filter scheme. Subscript 'k' represents the current time step. Hat notation is used for calculated variables and uppercase '-' is for predicted variables.

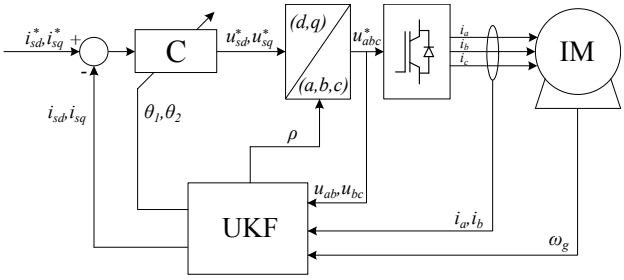

Fig. 11. Field-oriented control loop with dual unscented Kalman filter ('UKF'). Block 'C' represents the controller, block 'IM' is the squirrel-cage induction machine. Variables denoted with uppercase star '' are reference values.*

sponding L_{ld} and L_{lq}) is completely determined with θ_1 (related to γ) and θ_2.

This way, only asymmetries with the period that corresponds to doubled frequency of the flux rotation are respected in operation. For this case, this refers to the stator-isolation-fault-induced asymmetry and the saturation saliency inherent one.

8 SIMULATION RESULTS

This section provides simulation results for a 700 kW MATLAB/Simulink variable-speed variable-pitch wind turbine model with a two-pole 5.5 kW SCIG scaled to match the torque and power of 700 kW machine.

Generator parameters are: $L_s = L_r = 0.112$ H, $L_m = 0.11$ H, $R_s = 0.3304\ \Omega$, $R_r = 0.2334\ \Omega$ and PI controller gain is $K_r = 10$. Turbine parameters are: $C_{Pmax} = 0.4745$, $R = 25$ m, $\lambda_{opt} = 7.4$, $\omega_n = 29$ rpm, $T_{tn} = 230.5$ kNm with gearbox ratio $n_s = 105.77$. Stator flux rated value is $\psi_{sn} = 0.625$ Wb and sample time is chosen $T_s = 2 \cdot 10^{-4}$ s. Moment of inertia of wind turbine and generator, reduced to the generator side is $J = 72.11\ \mathrm{kgm}^2$. Due to minor influence, inverter dynamics are neglected in simulations.

In the sequel simulation results with diagnosed fault and $\left|\frac{\mathrm{d}\psi_{sx}}{\mathrm{d}t}\right| = k = 100$ Wb/s are presented. The stator flux is manipulated only by i_{sd} as presented in Fig. 12. The i_{sq} current is modulated to compensate the variations in i_{mr} due to rapid changing of i_{sd} in order to maintain the smooth torque as shown in Fig. 17. Torque ripple occurs only due to measurement noise included in simulations.

Stator flux amplitude envelope from (23) is shown in Fig. 13 and corresponding stator flux waveforms in phases a, b, c are shown in Fig. 15. Following from figures, the required restriction formed as described triangular waveform is satisfied in shorted phase (phase a). Phase currents calculated to achieve desired flux waveforms are shown in Fig. 14. Currents follow a sinusoidal shape with deviations at peak values. With better tracking performance of i_{sd} with respect to the reference value in Fig. 12 or by compensation of the reference value with included prediction procedure, more symmetric waveforms of flux, as well as those of currents, in phases a, b, c can be achieved.

Fig. 16 shows flux derivatives in all three phases. The figure shows that flux-derivative in the faulty phase never exceeds the imposed limit of $k = 100$ Wb/s.

Possible operating areas for different FTC approaches (from Fig. 5) are presented in Fig. 18. Maximum attainable power production for $k = 100$ Wb/s is approximately: 164 kW for *Faulty A*, 241 kW for *Faulty B* and 318 kW for *Faulty C* approach. Increase in power production with proposed flux modulation is evident.

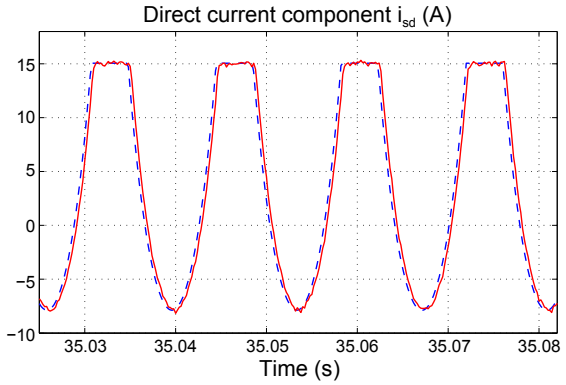

Fig. 12. Direct current component. Dashed line is reference value.

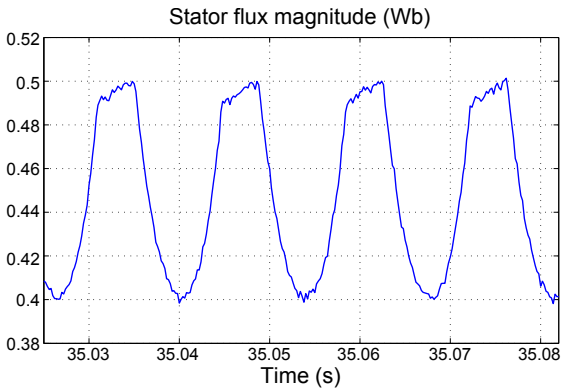

Fig. 13. Stator flux magnitude $|\psi_s|(t)$

9 CONCLUSION

A fault-tolerant control strategy for variable-speed variable-pitch wind turbines is introduced. The focus is on a squirrel-cage generator with diagnosed short-circuit between turns of the same phase on the stator. An extension

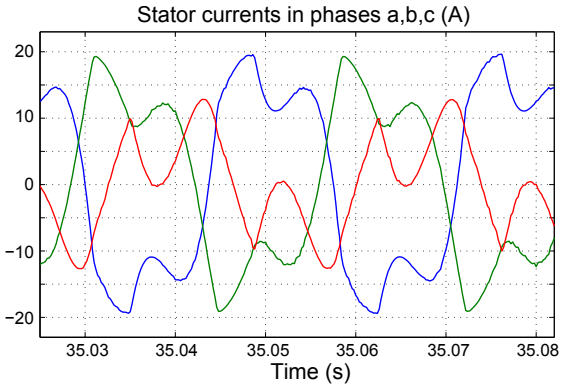

Fig. 14. Stator phase currents

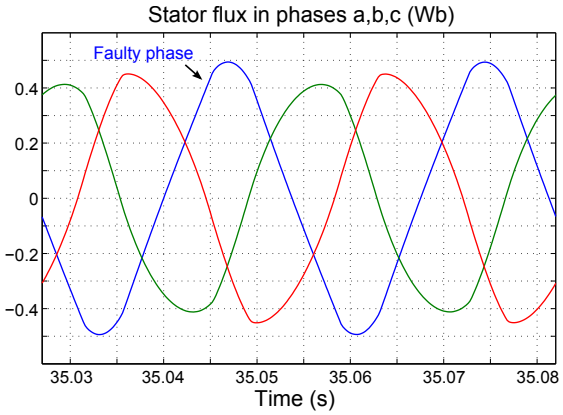

Fig. 15. Stator flux in phases a, b, c

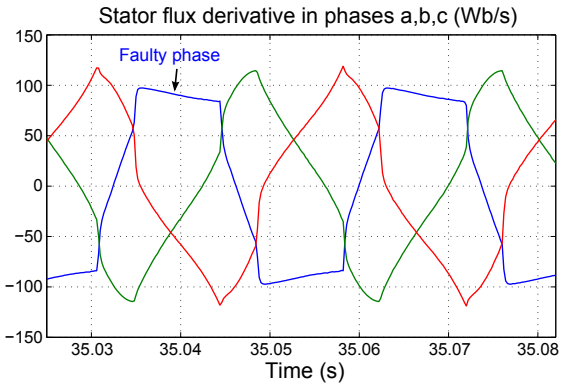

Fig. 16. Stator flux derivative in phases a, b, c

of the conventional wind turbine control structure is proposed that prevents the fault propagation and enables faulty wind turbine operation with reduced power. The power delivery under fault is deteriorated as less as possible compared to healthy machine conditions. Conventional field-oriented control is extended to achieve smooth operation regardless of fault-induced asymmetries.

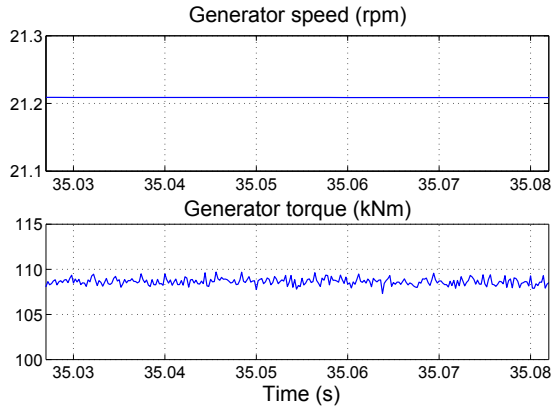

Fig. 17. Generator rotational speed and torque on the wind turbine rotor side

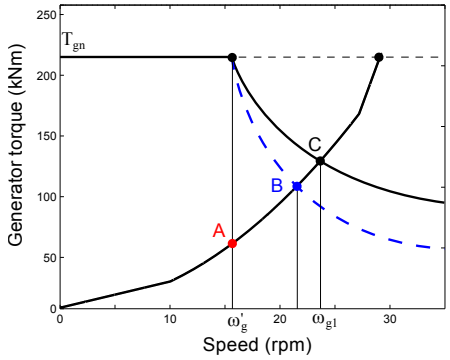

Fig. 18. Possible operating areas for different FTC approaches

ACKNOWLEDGEMENT

The research leading to these results has received funding from the European Community's Seventh Framework Programme under grant agreement no 285939 (ACROSS) and from the European Commission and the Republic of Croatia under grant FP7-SEE-ERA.net PLUS ERA 80/01, project MONGS - Monitoring of Wind Turbine Generator Systems.

REFERENCES

[1] Renewable Energy Policy Network for the 21st Century (REN21), "Renewables 2012," Global status report, 2012.

[2] S. Pourmohammad, A. Fekih, "Fault-Tolerant Control of Wind Turbine Systems - A Review",*Proc. of the 2011. IEEE Green Technologies Conference (IEEE-Green)*, April 2011.

[3] Z. Daneshi-Far, G. A. Capolino, H. Henao, "Review of Failures and Condition Monitoring in Wind Turbine Generators", *XIX International Conference on Electrical Machines - ICEM 2010*, September 2010.

[4] V. Lešić, M. Vašak, N. Perić, T. M. Wolbank and G. Joksimović, "Fault-Tolerant Control of a Blade-pitch Wind Turbine With Inverter-fed Generator", *20th IEEE International*

Symposium on Industrial Electronics, ISIE, pp. 2097-2102, June 2011.

[5] V. Lešić, M. Vašak, N. Perić, T. M. Wolbank and G. Joksimović, "Fault-Tolerant Control of a Wind Turbine With a Squirrel-cage Induction Generator and Rotor Bar Defects", *17th International Conference on Electrical Drives and Power Electronics, EDPE*, pp. 364-369, Sept. 2011.

[6] A. H. Bonnet and C. Yung, "Increased efficiency versus increased reliability," *IEEE Industry Applications Magazine*, vol.14, no.1, pp. 29-36, 2008.

[7] T. M. Wolbank, K. A. Loparo and R. Wöhrnschimmel, "Inverter Statistics for Online Detection of Stator Asymmetries in Inverter-Fed Induction Motors," *IEEE Transactions on Industry Applications*, vol.39, no.4, pp. 1102-1108, Jul./Aug. 2003.

[8] H. Oraee, "On-line detection of interturn voltage failures in electrical machine windings," *Proceedings of ICEM 1996*, vol.2, Vigo, Spain, pp. 440-445, 1996.

[9] O. Thorsen and M. Dalva, "A survey of faults on induction motors in offshore oil industry, petrochemical industry, gas terminals, and oil refineries," *IEEE Transactions on Industry Applications*, vol.31, pp. 1186-1196, Sept./Oct. 1995.

[10] G. Stojičić, G. Joksimović, M. Vašak, N. Perić and T. M. Wolbank, "Increasing Sensitivity of Stator Winding Short Circuit Fault Indicator in Inverter Fed Induction Machines," *15th International Power Electronics and Motion Control Conference, EPE-PEMC ECCE Europe 2012*, pp. DS2a.10-1–6, Sept. 2012.

[11] IEEE Committee Report, "Report of large motor reliability survey of industrial and commercial installation, Part I and Part II," *IEEE Transactions on Industry Applications*, vol.21, no.4, pp. 853-872, 1985.

[12] V. Lešić, M. Vašak, M. Gulin, N. Perić, G. Joksimović and T. M. Wolbank, "Field-oriented Control of an Induction Machine with Winding Asymmetries," *15th International Power Electronics and Motion Control Conference, EPE-PEMC 2012 ECCE Europe*, pp. LS7b-1.2-1–7, Sept. 2012.

[13] V. Lešić, M. Vašak, N. Perić, T. M. Wolbank and G. Joksimović, "Fault-Tolerant Control of a Wind Turbine With a Squirrel-cage Induction Generator and Rotor Bar Defects", *Automatika – Journal for Control, Measurement, Electronics, Computing and Communications*.

[14] L. Y. Pao and K. E. Johnson, "Control of Wind Turbines: Approaches, Challenges, and Recent Developments", *IEEE Control Systems Magazine* vol. 31, no. 2, pp. 44-62, April 2011.

[15] F. D. Bianchi, H. De Battista and R. J. Mantz, *Wind Turbine Control Systems - Principles, Modelling and Gain Scheduling Design.*, London, England: Springer, ISBN 1-84628-492-9, 2007.

[16] T. Burton, D. Sharpe, N. Jenkins and E. Bossanyi *Wind Energy Handbook*, England: John Wiley & Sons, ISBN 0-471-48997-2, 2001.

[17] F. Blaabjerg, F. Iov, R. Teodorescu and Z. Chen. "Power Electronics in Renewable Energy Systems" *Proc. of the 12th International Power Electronics and Motion Control Conf. (EPE-PEMC 2006)*, 2006.

[18] W. Leonhard, *Control of Electrical Drives*, Berlin, Germany: Springer Verlag, ISBN 3-540-41820-2, 2001.

[19] M. P. Kazmierkowski, F. Blaabjerg and R. Krishnan, *Control in Power Electronics - Selected Problems*, San Diego, California: Academic Press, An imprint of Elsevier Science, ISBN 0-12-402772-5, 2002.

[20] B. K. Bose, *Modern Power Electronics and AC Drives*, Upper Saddle River: Prentice-Hall, ISBN 0-13-016743-6, 2002.

[21] S. J. Julier and J. K. Uhlmann, *A general method for approximating nonlinear transformations of probability distributions*, Technical report, Dept. of Engineering Science, University of Oxford, November 1996.

[22] S. Haykin (Editor), *Kalman Filtering and Neural Networks*, New York: John Wiley & Sons, ISBN 0-471-36998-5, 2001.

[23] M. Vašak, M. Baotić, I. Petrović and N. Perić, "Electronic Throttle State Estimation and Hybrid Theory Based Optimal Control", *Proceedings of the IEEE International Symposium on Industrial Electronics ISIE 2004*, pp. 323-328, May 2004.

[24] E. Ivanjko, I. Petrović and M. Vašak, "Sonar-based Pose Tracking of Indoor Mobile Robots", *Automatika - Journal for control, measurement, electronics, computing and communications*, vol. 45, no. 3-4, pp. 145-154, 2004.

[25] M. Doumiati, A. Victorino, A. Charara and D. Lechner, "Onboard Real-Time Estimation of Vehicle Lateral Tire–Road Forces and Sideslip Angle", *IEEE/ASME Transactions on Mechatronics*, vol. 16, no. 4, pp. 601-614, 2010.

[26] M. Pacas, "Sensorless Drives in Industrial Applications", *IEEE Industrial Electronics Magazine* vol. 5, no. 2, pp. 16-23, June 2011.

[27] J. Holtz, "Perspectives of Sensorless AC Drive Technology From the State of the Art to Future Trends", *Proc. of the PCIM Europe*, Nürnberg, Germany, pp. 80-87, June 2005.

[28] G. Stojičić, P. Nussbaumer, G. Joksimović, M. Vašak, N. Perić and T. M. Wolbank, "Precise Separation of Inherent Induction Machine Asymmetries from Rotor Bar Fault Indicator", *8th IEEE International Symposium on Diagnostics for Electrical Machines, Power Electronics & Drives, SDEMPED*, 2011.

[29] T. M. Wolbank, P. Nussbaumer, Hao Chen and P. E. Macheiner, "Monitoring of Rotor-Bar Defects in Inverter-Fed Induction Machines at Zero Load and Speed," *IEEE Transactions on Industrial Electronics*, vol.58, no.5, pp. 1468-1478, May. 2011.

[30] M. Barut, S. Bogosyan and M. Gokasan, "Experimental Evaluation of Braided EKF for Sensorless Control of Induction Motors", *IEEE Transactions on Industrial Electronics*, vol.55, no.2, pp. 620-632, Feb. 2008.

Vinko Lešić received his master degree in electrical engineering and information technology from University of Zagreb Faculty of Electrical Engineering and Computing (UNIZG-FER) in 2010. Currently, he is with the Department of Control and Computer Engineering at UNIZG-FER where he is pursuing his PhD degree. His research interests are in the area of control theory with application to advanced control of electrical drives and wind turbine generators.

Mario Vašak is an Assistant Professor at the Department of Control and Computer Engineering of University of Zagreb Faculty of Electrical Engineering and Computing (UNIZG-FER). He received his PhD degree in Electrical Engineering from UNIZG-FER in 2007. He works in the areas of predictive/robust/fault-tolerant control and computational geometry applied to them, in the following application domains: renewable energy systems, water management systems, energy-efficient buildings, energy-efficient railway transportation and automotive systems. On behalf of UNIZG-FER he led an FP7-SEE-ERA.net PLUS research project MONGS on generator-fault-tolerant control in wind turbines, and currently he is UNIZG-FER leader of the FP7-STREP UrbanWater that deals with fresh water supply system management in urban environments. He published over 40 papers in journals and conference proceedings.

Nedjeljko Perić received the B.Sc., M.Sc. and Ph.D. degrees in Electrical Engineering from the University of Zagreb Faculty of Electrical Engineering and Computing (UNIZG-FER) in 1973, 1980, and 1989, respectively. From 1973 to 1993 he worked at the Institute of Electrical Engineering of the Končar Corporation, Croatia, as an R&D engineer, Head of the Positioning Systems Department, and Manager of the Automation Section. In 1993 he joined the Department of Control and Computer Engineering at FER Zagreb as an associate professor. He was appointed as a full professor in 1997 and since 2010 he serves as UNIZG-FER dean. His current research interests are in the fields of process identification and advanced control techniques. In periods 1992-1998 and 2000-2011 he served as the Chairman of KoREMA, the Croatian Society for Communications, Computing, Electronics, Measurements and Control. He is also a member of several international professional associations. Professor Perić is a Fellow of Croatian Academy of Engineering.

Gojko M. Joksimović received PhD degree and the Full Professor degree from University of Montenegro, Montenegro, in 2000 and 2011, respectively. His main research areas include analysis of electrical machines, condition monitoring of electrical machines, and power electronics and control. He is the author of a few books and more than 50 papers published in leading international scientific journals and international conferences.

Thomas M. Wolbank received the doctoral degree and the Habilitation from Vienna University of Technology, Vienna, Austria, in 1996 and 2004, respectively. Currently, he is with the Department of Energy Systems and Electrical Drives, Vienna University of Technology, Vienna, Austria. He has co-authored some 100 papers in refereed journals and international conferences. His research interests include saliency-based sensorless control of AC drives, dynamic properties and condition monitoring of inverter-fed machines, transient electrical behavior of AC machines, and motor drives and their components and controlling them by the use of intelligent control algorithms.

AUTHORS' ADDRESSES

Vinko Lešić, M.Sc.
Asst. Prof. Mario Vašak, Ph.D.
Prof. Nedjeljko Perić, Ph.D.
Department of Control and Computer Engineering,
Faculty of Electrical Engineering and Computing,
University of Zagreb,
Unska 3, HR-10000, Zagreb, Croatia
email: {vinko.lesic,mario.vasak,nedjeljko.peric}@fer.hr

Prof. Gojko M. Joksimović, Ph.D.
Faculty of Electrical Engineering,
University of Montenegro,
Džordža Vašingtona bb, ME-81000, Podgorica, Montenegro
email: joxo@ac.me

Prof. Thomas M. Wolbank, Ph.D.
Institute of Energy Systems and Electrical Drives,
Faculty of Electrical Engineering and Information Technology,
Vienna University of Technology,
Gusshausstrasse 25/370-2, AT-1040, Vienna, Austria
email: thomas.wolbank@tuwien.ac.at

Received: 2012-07-17
Accepted: 2012-10-15